The influence of imperfections on the flow structure of steady vortex breakdown bubbles

MORTEN BRØNS[1], WEN ZHONG SHEN[2], JENS NØRKÆR SØRENSEN[2] AND WEI JUN ZHU[1,2]

[1]Department of Mathematics, Technical University of Denmark, DK-2800 Lyngby, Denmark

[2]Department of Mechanics, Technical University of Denmark, DK-2800 Lyngby, Denmark

Vortex breakdown bubbles in the flow in a closed cylinder with a rotating end-cover have previously been successfully simulated by axisymmetric codes in the steady range. However, high-resolution experiments indicate a complicated open bubble structure incompatible with axisymmetry. Numerical studies with generic imperfections in the flow have revealed that the axisymmetric bubble is highly sensitive to imperfections, and that this may resolve the apparent paradox. However, little is known about the influence of specific, physical perturbations on the flow structure. We perform fully three-dimensional simulations of the flow with two independent perturbations: an inclination of the fixed cover and a displacement of the rotating cover. We show that perturbations below a realistic experimental uncertainty may give rise to flow structures resembling those obtained in experiments, that the two perturbations may interact and annihilate their effects, and that the fractal dimension associated with the emptying of the bubble can quantitatively be linked to the visual bubble structure.

1. Introduction

The flow in a closed cylindrical container driven by a rotating end-cover has long been a basic set-up for the study of recirculation zones on a main vortex, also known as vortex breakdown of bubble type (Leibovich 1984). Vogel (1968) and Ronnenberg (1977) made the first experimental investigations and Escudier (1984) identified flow regimes with one, two, or three steady breakdown bubbles and mapped an experimental bifurcation diagram in terms of the two dimensionless parameters of the problem, the Reynolds number Re and the aspect ratio h of the cylinder,

$$Re = \frac{\Omega R^2}{\nu}, \quad h = \frac{H}{R}. \tag{1}$$

Here, Ω is the angular velocity of the rotating end-cover, R is the radius of the cylinder, H is the height, and ν is the kinematic viscosity of the fluid.

When the flow is steady it appears axisymmetric, and numerous numerical solutions of the Navier–Stokes equations assuming axisymmetry (Lugt & Abboud 1987; Lopez 1990; Daube 1991; Tsitverblit 1993; Gelfgat, Bar-Yoseph & Solan 1996; Brøns, Voigt & Sørensen 1999) reproduce the number, shape, and location of the breakdown bubbles very well.

The axisymmetry of the flow is consistent with the three-dimensional computational stability analysis of Gelfgat, Bar-Yoseph & Solan (2001). For aspect ratios h around

the value we consider here, it was shown that the steady axisymmetric flow is linearly stable to all perturbations. The first loss of stability of this solution occurs in a Hopf bifurcation to an axisymmetric mode, and asymmetric modes appear only far away from the steady regime. The stability analysis agrees with the pseudo-spectral computations of Serre & Bontoux (2002) at a high aspect ratio, where, in the steady domain, higher modes die out as transients and leave an axisymmetric flow.

After the loss of stability of the steady flow a number of interesting dynamical phenomena involving interactions of Hopf bifurcations and transition to quasi-periodic states have been found numerically under the assumption of axisymmetry. Experimental studies have confirmed the numerical predictions (Stevens, Lopez & Cantwell 1999; Lopez, Cui & Lim 2006). Hence, on the Eulerian level, the flow in the cylinder is very well described by the axisymmetric Navier–Stokes equations in a quite large range of the parameters h and Re. However, on the Lagrangian level things are different. High-resolution visualization experiments by Spohn, Mory & Hopfinger (1998) show a complicated folded and asymmetric structure of the downstream part of the steady bubble which is incompatible with the assumption of an axisymmetric velocity field. A prominent difference is that in steady axisymmetric flow the breakdown bubble must be closed, while the experimentally observed asymmetric bubbles are open and exchange fluid with the main vortex. As visualization experiments are an important means to obtain information about the spatial structures in the flow, and transport of particles is of interest in understanding the mixing properties of the flow, it is worthwhile to study the Lagrangian structure of the breakdown zones.

Several researchers have addressed the fundamental inconsistency between computations and experiments in the steady regime. Gelfgat (2002) has pointed out that if the density difference between tracer particles and the fluid is taken in account, the particle paths will be asymmetric, even if the flow field is axisymmetric. This may result in a misleading picture of the flow field in a visualization experiment. However, numerical simulations including this effect do not result in particle traces which resemble the experimentally obtained patterns in the steady regime.

A series of papers by Sotiropoulos and coworkers (Sotiropoulos & Ventikos 1998, 2001; Sotiropoulos, Ventikos & Lackey 2001; Sotiropoulos, Webster & Lackey 2002) has revealed the extreme sensitivity of the flow to imperfections. Fully three-dimensional simulations are performed on a curvilinear grid which does not comply with the rotational symmetry of the problem. On the Eulerian level, the simulations give results which are axisymmetric to a high degree of precision. On the Lagrangian level, however, the small imperfections induced by the grid suffice to give a clearly asymmetric flow structure, with particle traces closely resembling the experimental results by Spohn *et al.* (1998).

The effect of external perturbations was studied by Ventikos (2002) who replaced the circular cross-section of the flow domain by a slightly eccentric ellipse. Asymmetric and complex streamlines were also obtained, even for very small eccentricities. The details of the bubble structure did not, however, resemble the experimental ones. Similarly, Thompson & Hourigan (2003) mimicked computationally the effect of a misalignment of the rotating cover. The axisymmetric flow domain was retained, and asymmetric boundary conditions on the rotating cover were applied as an approximate model of the misalignment. Very small misalignments gave rise to clearly asymmetric bubble structures, resembling those obtained by Spohn *et al.* (1998).

Hence, little is known about the influence of specific, realistic perturbations of the flow as they may be applied intentionally or as unavoidable imperfections in

an experiment. To elucidate the sensitivity of the flow to external perturbations we perform in the present paper fully three-dimensional simulations of the flow with two simple, independent perturbations: an inclination of the fixed cover and a displacement of the axis of rotation of the rotating cover. We will show, on one hand, that for a relatively large controlled inclination of the fixed cover, the experimentally obtained flow structure is very well reproduced, and, on the other hand, that perturbations below a realistic experimental uncertainty can reproduce the experimental results by Spohn *et al.* (1998) in an axisymmetric set-up. Furthermore, we will show that the two independent perturbations may interfere constructively or destructively with regard to the openness of the bubble, and that this can be understood from the Melnikov theory of perturbed heteroclinic connections. Finally, we compute the fractal dimension associated with the devil's staircase appearing when the emptying of particles from the bubble is monitored, and show how this number matches the openness of the bubble as it appears in visualizations.

2. Topology of vortex breakdown bubbles

Holmes (1984) has identified the basic features of the Lagrangian dynamics when an axisymmetric vortex breakdown bubble is perturbed. See also Sotiropoulos *et al.* (2001) and Hartnack, Brøns & Spohn (2000). Here we briefly review the theory.

For a given steady three-dimensional velocity field in Cartesian coordinates

$$\boldsymbol{v} = (u(x, y, z), v(x, y, z), w(x, y, z)) \tag{2}$$

the streamlines are found by solving the differential equations

$$\frac{\mathrm{d}x}{\mathrm{d}t} = u(x, y, z), \quad \frac{\mathrm{d}y}{\mathrm{d}t} = v(x, y, z), \quad \frac{\mathrm{d}z}{\mathrm{d}t} = w(x, y, z), \tag{3}$$

for $\boldsymbol{x}(t) = (x(t), y(t), z(t))$. In a visualization experiment massless tracer particles follow the streamlines, so the structure of the solution curves of equations (3) is of interest here. This is conveniently described with concepts from low-dimensional nonlinear dynamics.

An axisymmetric recirculating bubble is characterized by the presence of stagnation points (or critical points) on the axis, that is, points where $\boldsymbol{v} = \boldsymbol{0}$.

The top stagnation point P is of saddle type with invariant stable and unstable manifolds. The stable manifold $W^s(P)$ is defined as the set of streamlines $\boldsymbol{x}(t)$ for which $\boldsymbol{x}(t) \to P$ for $t \to \infty$. This manifold is one-dimensional, and consists of a part of the axis. The unstable manifold $W^u(P)$ consists of the streamlines $\boldsymbol{x}(t)$ with $\boldsymbol{x}(t) \to P$ for $t \to -\infty$. It constitutes a two-dimensional streamsurface emanating from from P. Similarly, the bottom stagnation point Q has stable and unstable manifolds. Owing to axisymmetry $W^u(P) = W^s(Q)$, and this closed surface constitutes the bubble surface. Similarly, the part of the cylinder axis inside the bubble belongs to both $W^s(P)$ and $W^u(Q)$. See figure 1(*a, b*). If tracer particles are released close to the axis above P, they will spiral around $W^s(P)$ down towards P and then out along $W^u(P)$. This surface is attracting as the vector field in directions transverse to it points toward the surface. Hence, small variations in the initial conditions of tracer particles will quickly be damped out, and an accurate visualization of $W^u(P)$ is obtained.

If the velocity field $\boldsymbol{v}$ is perturbed by an imperfection, for example in the geometry of the flow domain such that the flow is no longer axisymmetric, changes in the bubble structure will occur. Stagnation points of saddle type are structurally stable, i.e. they may move slightly, but retain their local structure with stable and unstable manifolds
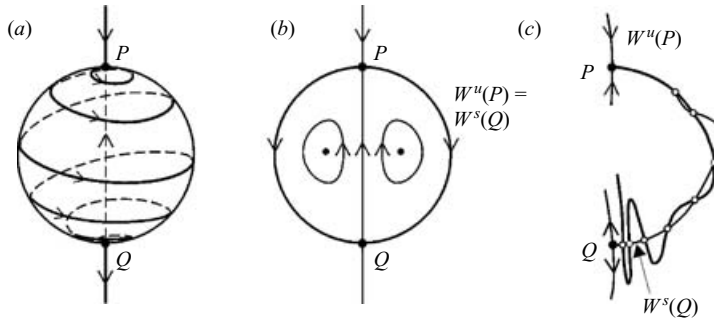
FIGURE 1. Qualitative sketches of vortex breakdown bubble shapes. (*a*) A closed axisymmetric breakdown bubble surface. A heteroclinic streamline connecting P and Q is shown. (*b*) Intersection of the axisymmetric bubble with a meridional plane. (*c*) Bubble structure in the perturbed case. For clarity, only the right-hand part is shown. The open circles indicate a part of a heteroclinic streamline at the intersection of $W^u(P)$ and $W^s(Q)$.

(Wiggins 1990). Tracer particles will still follow $W^u(P)$, and close to P the manifold will closely resemble the unperturbed case. The global structure, however, will be different. For an axisymmetric steady bubble, the surface $W^u(P) = W^s(Q)$ consists entirely of *heteroclinic streamlines*, that is, streamlines $x(t)$ with the property that $x(t) \to P$ for $t \to -\infty$ and $x(t) \to Q$ for $t \to \infty$. If the axisymmetry is broken, $W^u(P)$ and $W^s(Q)$ will no longer be identical, but some of the heteroclinic streamlines will persist. Figure 1(*c*) shows the situation in a meridional plane. A heteroclinic streamline appears as an infinite sequence of points, accumulating in backward time on P and in forward time on Q. Owing to the saddle point nature of Q, $W^u(P)$ is stretched as it approaches Q. Pieces of $W^u(P)$ between two heteroclinic points below $W^s(Q)$ are stretched downwards, and pieces above $W^s(Q)$ are stretched upwards inside the bubble. A similar folding and stretching of $W^s(Q)$ occurs as it approaches P in backward time. As only $W^u(P)$ is attracting, $W^s(Q)$ will not be seen in an experiment with tracer particles and only the folded structure of the downstream part of the bubble close to Q can be visualized. Even the smallest imperfection in an experiment will in principle give rise to open bubbles with a folded downstream part, shaped as shown in figure 1(*c*).

The present analysis only considers the outer bubble contour. In axisymmetric flow, the inside of the bubble is filled with closed streamsurfaces, as indicated on figure 1(*b*). An asymmetric perturbation will also have a profound influence on the flow inside the bubble. A detailed analysis is outside the scope of the present paper. We only mention that a complicated pattern of chaotic streamlines interspersed with islands of periodic behaviour will typically appear. See e.g. Wiggins (1990) and Sotiropoulos *et al.* (2001).

Transversal intersections of manifolds also occur when the flow is axisymmetric but time-periodic, where structures similar to figure 1(*c*) are found in the Poincaré plane (Lopez & Perry 1992*a,b*). Thus, in this case, there is also a complicated transport of fluid in and out of the breakdown bubble.

3. Numerical method

We use the cylinder radius R and the angular velocity Ω of the bottom cover to non-dimensionalize the system. In dimensionless variables, we hence consider a cylindrical container with radius 1 and height h filled with viscous fluid. The top cover
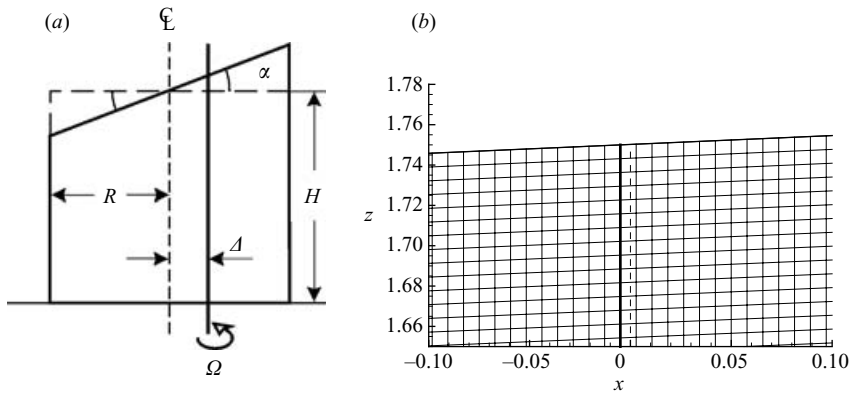
FIGURE 2. (*a*) Geometry of the system showing the inclination α of the fixed cover and the displacement Δ of the rotating bottom cover. (*b*) Part of the computational mesh in the azimuthal plane $\theta = 0$ close to the centre of the top cover for $\Delta = -0.5\%$ and $\alpha = 2.5°$. The axis of rotation is shown as a dark solid line and the cylinder axis is shown as a dashed line.

is inclined an angle α with the cylinder axis. The bottom cover rotates with constant angular velocity $\Omega = 1$. The axis of rotation is displaced a distance Δ from the cylinder axis. See figure 2(*a*). In the present paper we consider $Re = 1850$ and $h = 1.75$, as this is the case considered experimentally by Spohn *et al.* (1998) and several others. For this parameter combination a single large steady breakdown bubble exist.

The flow is governed by the incompressible Navier–Stokes equations. Because of the simple geometry of the cylinder, it is natural to formulate the equations in cylindrical coordinates (r, θ, z). The resulting three-dimensional Navier–Stokes equations are solved by a predictor–corrector method based on the cell-centred finite-volume/multi-block strategy of Michelsen (1992) and Sørensen (1995). In the predictor step, the momentum equations are discretized using a second-order backward differentiation scheme in time or pseudo-time (local time-steps for steady computations) and second-order central differences in space, except for the convective terms that are discretized by the QUICK upwind scheme. Since all variables are defined at cell centres, no special treatment is needed for the singularity problem at the centre axis. In the corrector step, the new Rhie–Chow interpolation developed by Shen, Michelsen & Sørensen (2001) and the new SIMPLEC scheme on collocated grids by Shen *et al.* (2003) are used in order to avoid numerical oscillations from pressure decoupling. The pressure Poisson equations are solved by a five-level multi-grid technique. For more details, the reader is referred to the original works.

Since the top cover is inclined with an angle α and the rotating axis is displaced by Δ ($\Delta \ll 1$) from the cylinder axis, the mesh is generated such that

$$\theta_j = 2\pi(j-1)/N_y,$$
$$r_{ij} = (1 - \Delta \cos \theta_j)(i-1)/N_x,$$
$$z_{ijk} = (h + r_{ij} \cos \theta_j \tan \alpha)(k-1)/N_z,$$

where $1 \leqslant i \leqslant N_x + 1$, $1 \leqslant j \leqslant N_y + 1$, and $1 \leqslant k \leqslant N_z + 1$. A detail of the mesh in the region close to the top centre is shown in figure 2(*b*). From the figure, we can see that the mesh is not orthogonal and the rotating axis (heavy line) is displaced from the cylinder axis (dashed line). Although the Navier–Stokes solver is capable of determining both steady and unsteady flow on non-orthogonal meshes, the steady
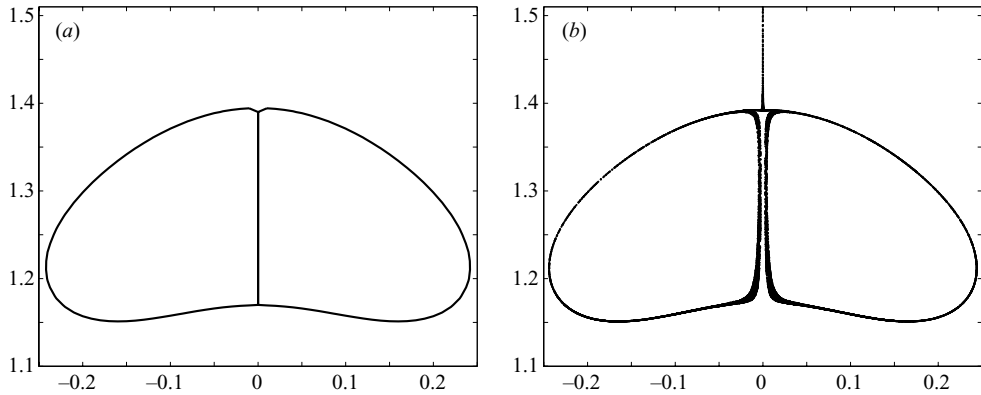
FIGURE 3. (a) The iso-curve $\psi = 0$ obtained from an axisymmetric simulation (Sørensen & Loc 1989; Daube 1991), representing the bubble surface. (b) Particle traces in the three-dimensional velocity field with axisymmetric geometry $\alpha = \Delta = 0$.

version is used in the current paper. The computational domain consists of $N_x = 128$ cells in the radial direction, $N_y = 128$ in the tangential direction and $N_z = 256$ in the axial direction. With this mesh and under axisymmetric conditions we get results which agree closely with the results obtained by an axisymmetric code (Sørensen & Loc 1989) which has been thoroughly validated.

In the velocity field $\boldsymbol{v}(\boldsymbol{x})$ the motion of massless tracer particles is simulated by solving the ordinary differential equations (3) numerically using MATLAB routines. The variable-order Adams–Bashforth–Moulton PECE solver *ode113* is used with a relative tolerance of 10^{-8}. The velocity field is computed in each cell by tri-linear interpolation with the routine *interp3*. In each experiment, 20 000 particles are released uniformly at circles with centres at the cylinder axis. The circles are placed at $z = 1.745$, well above the top stagnation point of the bubble which under axisymmetric conditions is at $z = 1.4$. The radii of the circles vary typically from 10^{-10} to 10^{-4}, and, as discussed in § 2, the results are insensitive to these choices.

We will consider particle positions after 50 revolutions of the cover by displaying the particles which are present in a thin sheet around the azimuthal plane $\theta = 0$. This corresponds to an experiment where particles are visualized by an azimuthal laser sheet.

To validate the three-dimensional solver, we compare with results from an axisymmetric simulation obtained from an axisymmetric Navier–Stokes code developed at LIMSI/CNRS (Sørensen & Loc 1989; Daube 1991). This is based on a stream-function/vorticity formulation, so streamlines are directly available as iso-curves of the streamfunction ψ. Figure 3(a) shows the iso-curve $\psi = 0$ which represents the breakdown bubble. Figure 3(b) shows a particle tracing experiment from the full three-dimensional simulation. Keeping in mind that the plot in figure 3(b) also contains inherent truncation errors from the integration, there is excellent agreement between the two plots.

As we use relaxation with pseudo-time steps to compute steady solutions no information about transient behaviour or stability of the solutions is obtained. However, since we consider small perturbations from an axisymmetric solution which is far from the stability limit, we expect, from continuity of eigenvalues with respect to parameters, that the steady solution maintains its stability. This is confirmed
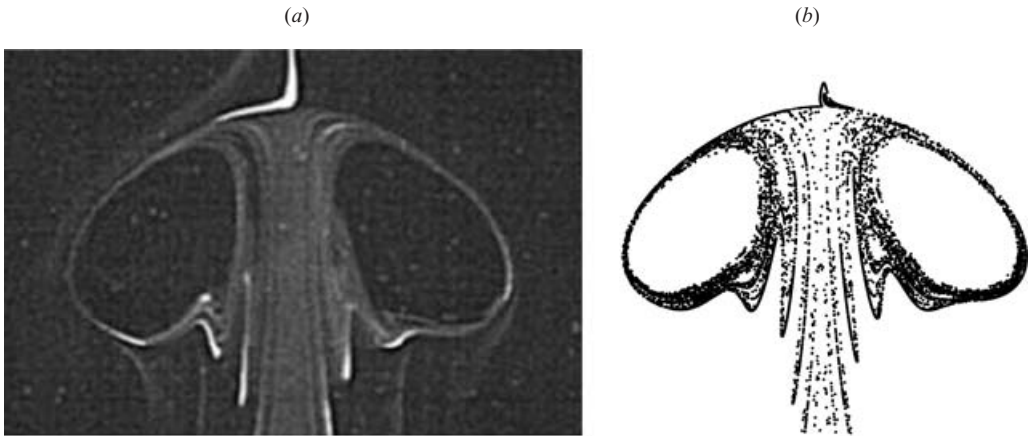
(*a*)　　　　　　　　　　　　　　　　　　(*b*)

FIGURE 4. (*a*) Experiment with inclination $\alpha = 0.4°$ from Sotiropoulos *et al.* (2002). (*b*) Computation with inclination $\alpha = 0.4°$, stretched 8 % vertically.

experimentally. Spohn *et al.* (1998), Sotiropoulos *et al.* (2002) and Lopez *et al.* (2006) all observe steady flow, even if the bubble structures show asymmetric structures stemming from experimental imperfections or a deliberate inclination of the fixed cover. Furthermore, Sørensen, Naumov & Mikkelsen (2006) confirm the numerical stability limits obtained numerically by Gelfgat *et al.* (2001) in a real experiment. Hence we are confident that the steady solutions we find are stable.

4. Comparison with experiments

To compare visualization experiments with computations, optical effects must be taken into account, as pictures may be stretched in a way depending specifically on the apparatus. We have compensated this by stretching the computational results shown in figures 4 and 6 axially. We have not attempted to estimate the correct stretching rate in each case, but have simply chosen it by fitting the upper bubble part to experiments.

Sotiropoulos *et al.* (2002) have performed experiments with a controlled inclination $\alpha = 0.4°$. This is compared with simulations of the bubble structure in figure 4. The general shape, amplitude, and spacing of the spikes of the folded downstream part of the bubble compare well. In contrast, on the Eulerian level, this inclination gives rise to an almost negligible asymmetry as shown in figure 5.

Figure 6(*a*) shows an experiment by Spohn *et al.* (1998), where great care has been taken to ensure an axisymmetric geometry. Nevertheless, the flow is clearly asymmetric. In figure 6(*b*) we show a simulation with a displacement of the axis of rotation $\Delta = -0.5$ % and obtain an almost identical bubble structure. Hence, as the radius of the cylinder in the experiment is 45.7 mm, a misalignment of the axis of rotation of only 0.23 mm suffices to give an effect of the same size as observed experimentally. We do not claim that this is the specific effect that causes the asymmetry in Spohn's experiment. As we shall see in figure 7, various combinations of α and Δ can give rise to almost identical bubble structures, and other imperfections may contribute as well. But the simulation demonstrates that an imperfection below a realistic experimental accuracy can explain the observed particle traces.
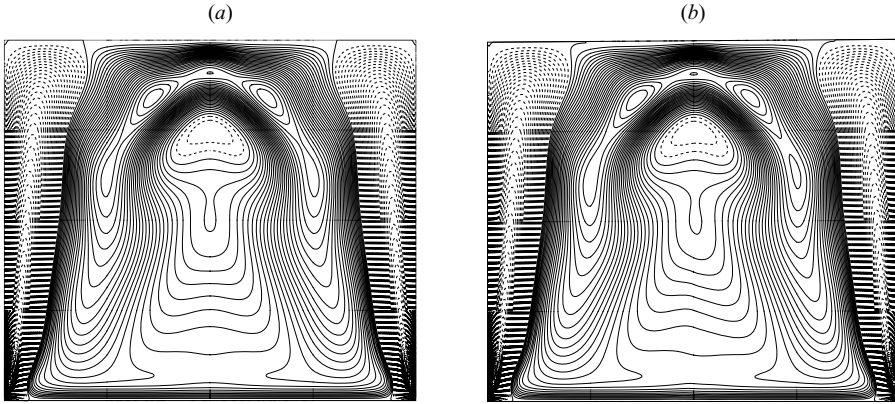
(*a*) (*b*)

FIGURE 5. Iso-curves of axial velocity w in a meridional section. The full lines represent upward velocities, the dashed lines are downward velocities. (*a*) Axisymmetric case. (*b*) Inclination of cover $\alpha = 0.4°$.
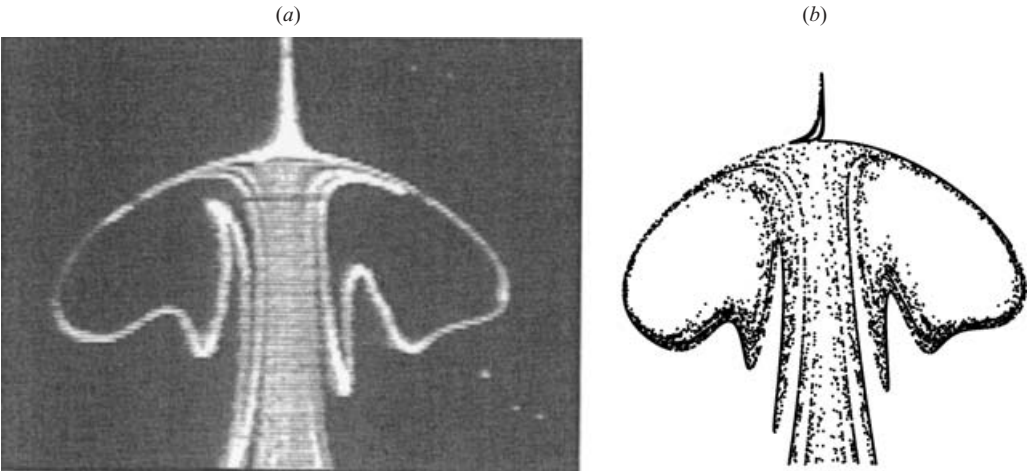
(*a*) (*b*)

FIGURE 6. (*a*) Experiment with $\alpha = 0$ from Spohn *et al.* (1998). (*b*) Computation with displacement $\Delta = -0.5\%$, stretched 12% vertically.

5. Interaction of perturbations

A series of particle tracing experiments with various values of α and Δ is shown in figure 7. It is clearly demonstrated that even very small imperfections result in open bubbles with folded downstream parts in agreement with the theory of § 2. It also appears that the two imperfections can interact to enhance or suppress their effect. For example, for $\alpha = 0.01°$, the folding of $W^u(P)$ is minimal for $\Delta = 0.01\%$.

This feature is clearly seen in figure 8, which shows particle traces for very small values of α and Δ. One can envisage a curve with positive slope in the (α, Δ) parameter plane corresponding to configurations with a minimal folding of the downstream part of the bubble.

An explanation can be obtained from the Melnikov perturbation theory of invariant manifolds (Guckenheimer & Holmes 1983; Wiggins 1990). Holmes (1984) has suggested using the Melnikov method to study the dynamics of vortex breakdown
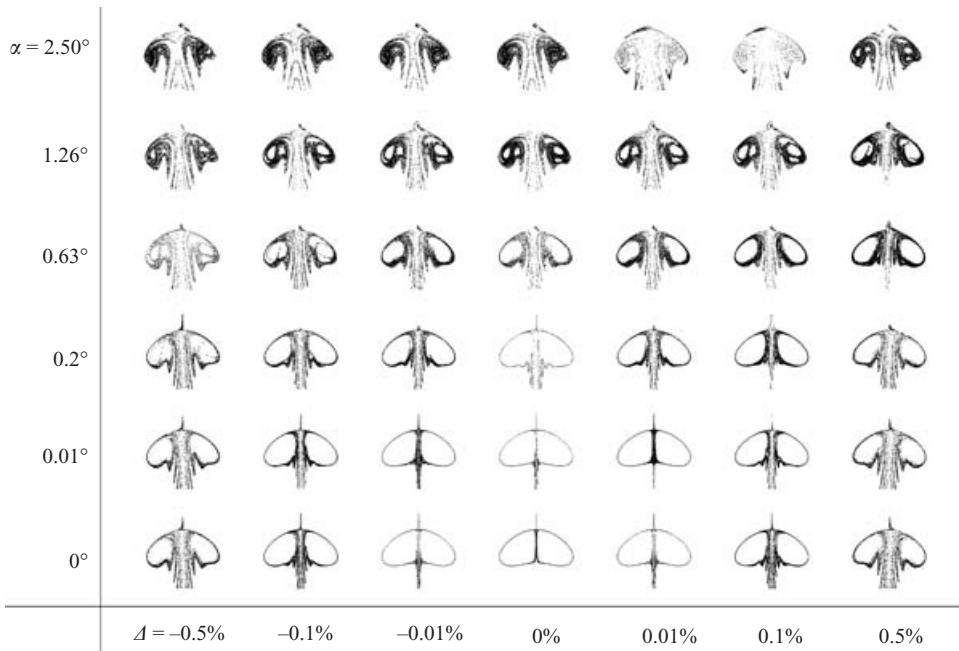
FIGURE 7. Particle traces for different values of the inclination α and the axis displacement Δ.
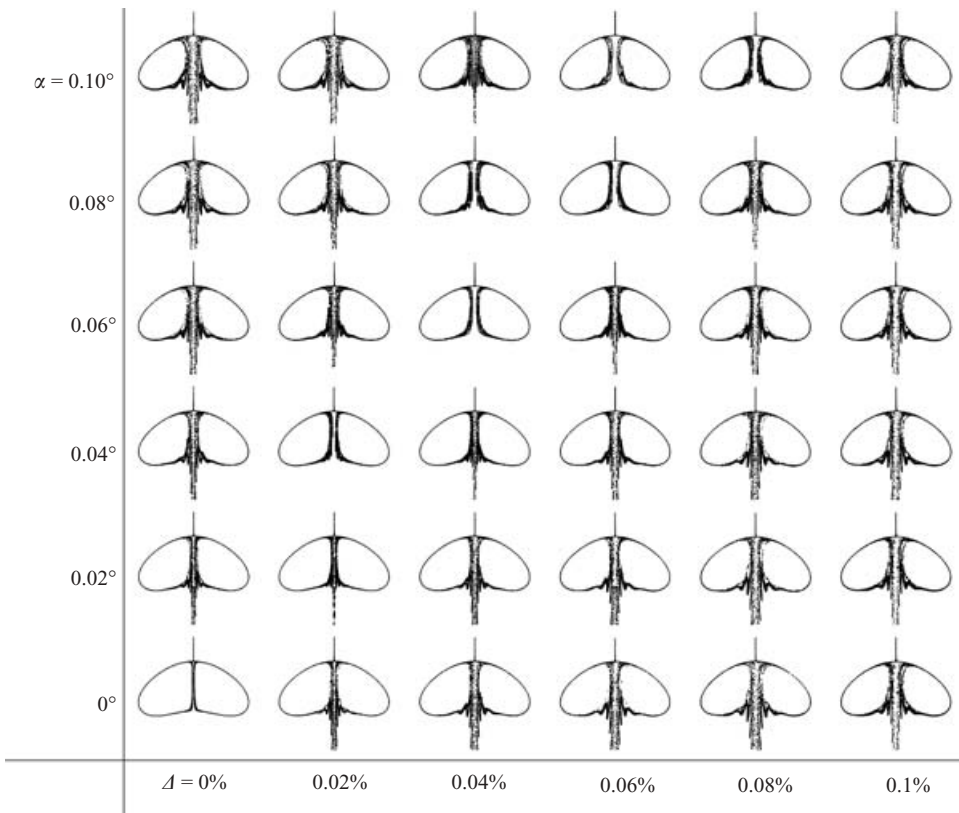

FIGURE 8. Further particle traces for small values of α and Δ.

in the periodic regime. From this theory, it is possible to compute an asymptotic measure of the distance between $W^u(P)$ and $W^s(Q)$, the *Melnikov function M*. The Melnikov function is defined along the unperturbed manifold $W^u(P) = W^s(Q)$. A zero of M corresponds to a point of intersection of $W^u(P)$ and $W^s(Q)$ as exemplified by the circles in figure 1(*c*).

In the present case, M will depend on the imperfection parameters α and Δ. Obviously, $M \equiv 0$ when $\alpha = \Delta = 0$, but there may be other combinations of α and Δ which make M identically zero. For such a combination, $W^u(P)$ and $W^s(Q)$ only differ to second order in the imperfection parameters and the folding of the manifolds will be minimal.

Rom-Kedar, Leonard & Wiggins (1990) performed an analytic derivation of the Melnikov function for a pair of oscillating vortices and found that the Melnikov function vanishes for certain non-zero combinations of the parameters defining the flow. Although a physically quite different problem, the streamline geometry is similar, and the periodic forcing corresponds to the angular symmetry here. As we only have the flow represented numerically, a similar analytical computation for the present problem is not possible, but could be performed numerically. However, Hartnack *et al.* (2000) computed the Melnikov function for a normal form model, where a simple analytical expression for the velocity field mimics the topology of a vortex breakdown bubble. Adding two generic imperfections, it was shown that at a certain ratio between the strengths of the imperfections, the Melnikov function vanishes, resulting in a minimal folding of the bubble surface.

6. Fractal dimension associated with emptying of the bubble

When the breakdown bubble is not closed, tracer particles may enter the bubble and stay there for a while before they exit close to the lower stagnation point Q. Sotiropoulos *et al.* (2001) studied the residence time of particles in the bubble, and found that the number of particles $NP(t)$ inside the bubble as a function of time t follows a devil's staircase. That is, the graph of NP consists of plateaus of varying length, and the set of 'holes' between the steps is a Cantor set with a fractal dimension d. It was found that $d = 0.4$, based on a flow where the asymmetry was generated by a computational mesh not being axisymmetric. Here we present computations of the fractal dimension in the case where the asymmetries are generated by physical imperfections.

The computations follow Sotiropoulos *et al.* (2001) and Bak (1986). Here we outline the method. Two thousand particles are randomly placed in a disk of radius 0.001 centred at the cylinder axis at $z = 1.74$, above the breakdown bubble. A particle is defined as being inside the bubble if it is above a horizontal plane just below the lower stagnation point of the bubble. All particles are released at $t = 0$, and $NP(t)$ is computed as the simulation progresses. A typical graph of NP is shown in figure 9(*a*). Periods with a constant number of particles inside the bubble alternate with bursts of particles leaving the bubble. A detailed view reveals a self-similar structure of a burst, which again consists of small periods with a constant number of particles interspersed with smaller bursts.

Let $T(r)$ denote the total width of plateaus of the graph of NP of width more than r, and let T_{max} be the maximum residence time in the simulation. If the space between the plateaus vanishes as a power function,

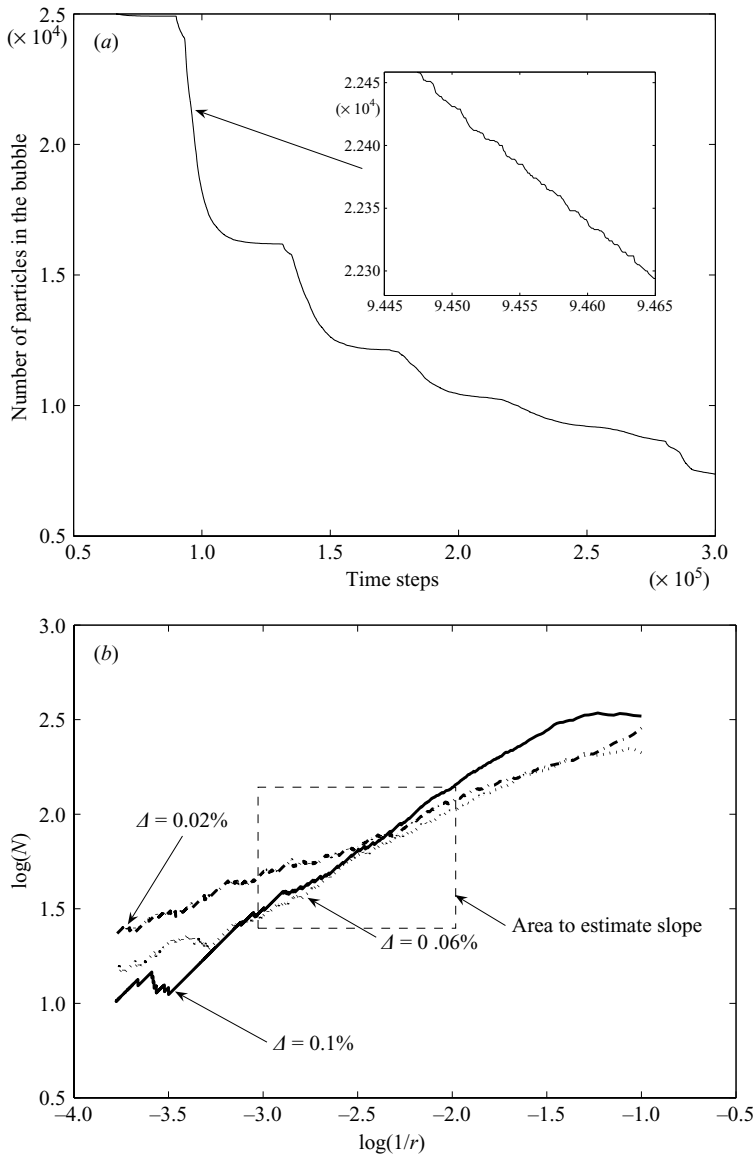$$T_{max} - T(r) \approx r^{1-d} \text{ as } r \to 0, \tag{4}$$

FIGURE 9. (a) Number of particles $NP(t)$ inside the bubble as a function of time t for $\alpha = 0.06°$, $\Delta = 0$. The graph displays a devil's staircase structure. (b) Sample graphs for $\alpha = 0.06°$ of $\log(N)$ vs. $\log(1/r)$, where N is defined in equation (5) and r is the length of plateaus in the staircase.

the fractal dimension of that set is d. Equivalently,

$$N(r) = \frac{T_{max} - T(r)}{r} \approx (1/r)^d. \tag{5}$$

Figure 9(b) shows sample graphs of N vs. $1/r$ on a log–log scale, where the exponent d is the slope of the linear relationship. Estimating d for $\alpha = 0.06°$ over two decades gives rise to the results shown in table 1. The cases treated are those shown in the third row of figure 8.

Δ	0%	0.02%	0.04%	0.06%	0.08%	0.1%
d	0.65	0.40	—	0.54	0.66	0.68

TABLE 1. Fractal dimension d of the Cantor set associated with particle emptying for $\alpha = 0.06°$ for different values of the axis displacement Δ, corresponding to the third row of figure 8. For $\Delta = 0.04\%$ no particles leave the bubble during the simulation, and d cannot be computed.

We observe a variation of d which follows the visual structure of the bubble: The more pronounced the folding of the bubble surface, the higher the value of d. For $\Delta = 0.04\%$, where the bubble is almost closed, the residence time of particles inside the bubble is so long that no particles leave during the simulation time, and d cannot be computed.

This behaviour is to be expected. When d is large, the steps of it NP are short, and the emptying process is more uniform in time. This is matched by a more 'spiky' bubble, where it is easier for particles to leave.

7. Conclusions

An axisymmetric vortex breakdown bubble is, using a notion from dynamical systems, *structurally unstable*. This means that arbitrarily small asymmetric perturbations of the velocity field will give rise to a fundamentally changed flow structure. This was pointed out by Holmes (1984) on a theoretical background and convincingly demonstrated by Sotiropoulos and co-workers who have obtained complicated asymmetric breakdown bubbles from the exceedingly small imperfections generated by an asymmetric computational grid. Whether this suffices to explain the experimentally observed asymmetric bubble structures is, however, another matter. Imperfections generated by a grid are not linked to any specific physical perturbation. Rather, they can be considered as a generic model for such imperfections, but one cannot infer the magnitude or nature of an external perturbation needed to provide the imperfection and whether such a perturbation is below a realistic experimental accuracy.

We have performed fully three-dimensional simulations of the flow in a cylinder with two external perturbations: an inclination of the fixed cover and a displacement of the axis of rotation. We have reproduced the flow structure obtained experimentally with an inclined cover, and have shown that a very small displacement of the axis of rotation can reproduce the experiments by Spohn *et al.* (1998). This shows that the structural instability of the axisymmetric bubble is indeed sufficient to explain the experimentally obtained asymmetry and no other physical mechanisms need to be invoked. We have shown that the independent perturbations may interact and result in bubbles that are almost closed as if they were axisymmetric, and have connected this to the Melnikov function from perturbation theory. From a physical point of view, this shows that one cannot deduce the nature of the perturbation in a given experiment from the structure of the bubble.

Finally, we have computed the fractal dimension related to the emptying of particles from the bubble as a function of the perturbation parameters. We have obtained a clear connection between the openness of the bubble and the fractal dimension, and hence a useful quantitative measure to describe the bubble structure.

REFERENCES

BAK, P. 1986 The Devil's staircase. *Physics Today* **39** (12), 38–45.

BRØNS, M., VOIGT, L. K. & SØRENSEN, J. N. 1999 Streamline topology of steady axisymmetric vortex breakdown in a cylinder with co- and counter-rotating end-covers. *J. Fluid Mech.* **401**, 275–292.

DAUBE, O. 1991 Numerical simulations of axisymmetric vortex breakdown in a closed cylinder. In *Vortex Dynamics and Vortex Methods* (ed. C. R. Anderson & C. Greengard). Lectures in Applied Mathematics, vol. 28, pp. 131–152. American Mathematical Society.

ESCUDIER, M. P. 1984 Observations of the flow produced in a cylindrical container by a rotating endwall. *Exps. Fluids* **2**, 189–196.

GELFGAT, A. Y. 2002 Three-dimensionality of trajectories of experimental tracers in a steady axisymmetric swirling flow: Effect of density mismatch. *Theor. Comput. Fluid Dyn.* **16**, 29–41.

GELFGAT, A. Y., BAR-YOSEPH, P. Z. & SOLAN, A. 1996 Stability of confined swirling flow with and without vortex breakdown. *J. Fluid Mech.* **311**, 1–36.

GELFGAT, A. Y., BAR-YOSEPH, P. Z. & SOLAN, A. 2001 Three-dimensional instability of axisymmetric flow in a rotating lid-cylinder enclosure. *J. Fluid Mech.* **438**, 363–377.

GUCKENHEIMER, J. & HOLMES, P. 1983 *Nonlinear Oscillations, Dynamical Systems, and Bifurcations of Vector Fields*. Springer.

HARTNACK, J. N., BRØNS, M. & SPOHN, A. 2000 The role of asymmetric perturbations in steady vortex breakdown bubbles. *DCAMM Report* 628. Technical University of Denmark.

HOLMES, P. 1984 Some remarks on chaotic particle paths in time-periodic, three-dimensional swirling flows. *Contemp. Maths* **28**, 393–404.

LEIBOVICH, S. 1984 Vortex stability and breakdown: Survey and extension. *AIAA J.* **22**, 1192–1206.

LOPEZ, J. M. 1990 Axisymmetric vortex breakdown part 1. Confined swirling flow. *J. Fluid Mech.* **221**, 533–552.

LOPEZ, J. M., CUI, Y. D. & LIM, T. T. 2006 Experimental and numerical investigation of the competition between axisymmetric time-periodic modes in an enclosed swirling flow. *Phys. Fluids* **18**, 104016.

LOPEZ, J. M. & PERRY, A. D. 1992*a* Axisymmetric vortex breakdown part 3. Onset of periodic flow and chaotic advection. *J. Fluid Mech.* **234**, 449–471.

LOPEZ, J. M. & PERRY, A. D. 1992*b* Periodic axisymmetric vortex breakdown in a cylinder with a rotating end wall. In *Gallery of Fluid Motion* (ed H. L. Reed). *Phys. Fluids* A **4**, 1869–1881.

LUGT, H. J. & ABBOUD, M. 1987 Axisymmetric vortex breakdown in a container with a rotating lid. *J. Fluid Mech.* **179**, 179–190.

MICHELSEN, J. A. 1992 Basis3D – a platform for development of multiblock PDE solvers. *AFM* 92-05. Department of Fluid Mechanics, Technical University of Denmark.

ROM-KEDAR, V., LEONARD, A. & WIGGINS, S. 1990 An analytical study of transport, mixing and chaos in an unsteady vortical flow. *J. Fluid Mech.* **214**, 347–395.

RONNENBERG, B. 1977 Ein selbstjustierendes 3-Komponenten-Laserdoppler-Anemometer nach dem Vergleichsverfaren, angewandt auf Untersuchungen in einer stationären zylindersymmetrischen Drehströmung mit einem Rückströmgebiet. Bericht 19. Max-Planck-Institut für Strömungsforschung, Göttingen.

SERRE, E. & BONTOUX, P. 2002 Vortex breakdown in a three-dimensional swirling flow. *J. Fluid Mech.* **459**, 347–370.

SHEN, W. Z., MICHELSEN, J. A., SØRENSEN, H. N. & SØRENSEN, J. N. 2003 An improved SIMPLEC method on collocated grids for steady and unsteady flow computations. *Numer. Heat Transfer* **B43** (3), 221–239.

SHEN, W. Z., MICHELSEN, J. A. & SØRENSEN, J. N. 2001 Improved Rhie-Chow interpolation for unsteady flow computations. *AIAA J.* **39** (12), 2406–2409.

SØRENSEN, J. N. & LOC, T. P. 1989 High-order axisymmetric Navier-Stokes code: Description and evaluation of boundary conditions. *Intl J. Numer. Meth. Fluids* **9**, 1517–1537.

SØRENSEN, J. N., NAUMOV, I. & MIKKELSEN, R. 2006 Experimental investigation of three-dimensional flow instabilities in a rotating lid-driven cavity. *Exps. Fluids* **41**, 425–440.

SØRENSEN, N. N. 1995 General-purpose flow solver applied over hills. RISØ-R-827-(EN). Risø National Laboartory.

SOTIROPOULOS, F. & VENTIKOS, Y. 1998 Transition from bubble-type vortex breakdown to columnar vortex in a confined swirling flow. *Intl J. Heat Fluid Flow* **19**, 446–458.

SOTIROPOULOS, F. & VENTIKOS, Y. 2001 The three-dimensional structure of confined swirling flows with vortex breakdown. *J. Fluid Mech.* **426**, 155–175.

SOTIROPOULOS, F., VENTIKOS, Y. & LACKEY, T. C. 2001 Chaotic advection in three-dimensional stationary vortex-breakdown bubbles: Šil'nikov's chaos and the devil's staircase. *J. Fluid Mech.* **444**, 257–297.

SOTIROPOULOS, F., WEBSTER, D. R. & LACKEY, T. C. 2002 Experiments on Lagrangian transport in steady vortex-breakdown bubbles in a confined swirling flow. *J. Fluid Mech.* **466**, 215–248.

SPOHN, A., MORY, M. & HOPFINGER, E. J. 1998 Experiments on vortex breakdown in a confined flow generated by a rotating disc. *J. Fluid Mech.* **370**, 73–99.

STEVENS, J. L., LOPEZ, J. M. & CANTWELL, B. J. 1999 Oscillatory flow states in an enclosed cylinder with a rotating endwall. *J. Fluid Mech.* **389**, 101–118.

THOMPSON, M. C. & HOURIGAN, K. 2003 The sensitivity of steady vortex breakdown bubbles in confined cylinder flows to rotating lid misalignment. *J. Fluid Mech.* **496**, 129–138.

TSITVERBLIT, N. 1993 Vortex breakdown in a cylindrical container in the light of continuation of a steady solution. *Fluid Dyn. Res.* **11**, 19–35.

VENTIKOS, Y. 2002 The effect of imperfections on the emergence of three-dimensionality in stationary vortex breakdown bubbles. *Phys. Fluids* **14** (3), L13–L16.

VOGEL, H. U. 1968 Experimentelle Ergebnisse über die laminäre Strömung in einem zylindriche Gehäuse mit darin rotierender Scheibe. Bericht 6. Max-Planck-Institut für Strömungsforschung, Göttingen.

WIGGINS, S. 1990 *Introduction to Applied Nonlinear Dynamical Systems and Chaos*. Springer.